Estuaries and Coasts (2024) 47:1799–1813
https://doi.org/10.1007/s12237-024-01342-x

SPECIAL ISSUE: WETLAND ELEVATION DYNAMICS

Elevation Changes in Restored Marshes at Poplar Island, Chesapeake Bay, MD: II. Modeling the Importance of Marsh Development Time

James T. Morris[1] · Lorie W. Staver[2]

Received: 21 July 2023 / Revised: 25 January 2024 / Accepted: 26 February 2024 / Published online: 15 April 2024
© The Author(s) 2024

Abstract

Tidal marshes in the Chesapeake Bay are vulnerable to the accelerating rate of sea-level rise (SLR) and subsidence. Restored and created marshes face the same risks as natural marshes, and their resilience to SLR may depend upon appropriate design and implementation. Here, the Coastal Wetland Equilibrium Model (CWEM) was used to assess the resilience of tidal marshes at the Paul S. Sarbanes Ecosystem Restoration Project at Poplar Island (PI) in mid-Chesapeake Bay, MD, where dredged material from navigation channels is being used to create new tidal marshes planted with *Spartina alterniflora* in the low marsh and *S. patens* in the high marsh. The site is microtidal with low inorganic sediment inputs, where the rate of marsh elevation change is dominated by the production of organic matter and, therefore, is proportional to net ecosystem production (NEP). The model demonstrated the importance of marsh development for surface elevation gain. In created marshes, the buildout of belowground biomass adds volume and results in faster growth of marsh elevation, but the gains slow as the marsh matures. Elevation gain is the lessor of the recalcitrant fraction of NEP sequestered in sediment or the rate of increase in accommodation space. Marshes can keep up with and fill accommodation space with sequestered NEP up to a tipping point determined by the rate of SLR. The PI low marsh platform was forecasted to drown in about 43 years after construction at the current rate of SLR. Marsh loss can be mitigated by periodic thin layer placement (TLP) of sediment. CWEM was used to simulate PI marsh responses to different TLP strategies and showed that there is an optimal design that will maximize carbon sequestration and resilience depending on the trajectory of mean sea level.

Keywords Sea level rise · CWEM · MEM · Salt marsh · Elevation gain · *Spartina alterniflora* · *Spartina patens* · Thin layer placement · Marsh development · Surface elevation table · Marsh restoration

Introduction

Historically, there were over 200 islands in the Chesapeake Bay (CB), ranging in scale from a few to hundreds of hectares (Cronin 2005). Many of the smaller islands have been lost due to natural and anthropogenic causes, including sea-level rise (SLR) since they were first mapped in the eighteenth century. These islands provided critical habitat for a variety of wildlife that require the protection from predators afforded by small, remote islands, including tidal marsh habitat. A large-scale project, the Paul S. Sarbanes Ecosystem Restoration Project at Poplar Island (Poplar Island), is replacing some of this lost habitat using material from maintenance dredging of the navigation channels in upper CB. Upon completion, the restoration site will provide 694 ha of habitat, including 314 ha of tidal marsh.

Although tidal marshes are vulnerable to SLR, they can adjust their surface elevation to keep pace with SLR, within limits (Morris et al. 2021). Through complex feedback resulting in the accumulation of organic and inorganic matter, they adjust to SLR by changes in their relative elevation (Morris et al. 2002), and their resilience is closely tied to elevation within the intertidal zone (Morris et al. 2022). The created tidal marshes at Poplar Island were designed as 80% low marsh (LM) and 20% high marsh (HM) (Maryland

Communicated by Mead Allison

✉ James T. Morris
jtmorris@baruch.sc.edu

Lorie W. Staver
lstaver@umces.edu

[1] Baruch Institute for Marine and Coastal Sciences, University of South Carolina, Columbia, SC 20208, USA

[2] University of Maryland Center for Environmental Science, Horn Point Laboratory, Cambridge, MD 21613, USA

Tidal Wetlands License Number 96-0728), a relatively high proportion of low marsh intended to maximize habitat value for fish. In anticipation of accelerating regional SLR due to global warming and local factors (Boesch et al. 2018), and in recognition that the Poplar Island 80/20 LM/HM ratio may not confer resilience to future rates of SLR, the ratio is currently being reconsidered. The research reported here was authorized to forecast the responses of the created marshes to rising water level and to determine the outcomes of different LM/HM ratios. We report simulation results of the Coastal Wetland Equilibrium Model (CWEM) adapted to marsh restoration at Poplar Island with two species, *Spartina alterniflora* and *S. patens*. The model output was compared to empirical measurements of marsh vertical accretion rates and parameterized using published literature and empirical measurements of elevation change, aboveground standing biomass, and belowground macro-organic matter.

Methods

Site Description

Poplar Island, located in mid-CB, is a large-scale habitat restoration project that serves as a placement site for dredged material from the navigation channels approaching Baltimore Harbor (U.S. Army Corps of Engineers 1996). The mean tide range is 0.34 m (NOAA Tides and Currents, station ID 8572271), and the mean surface salinity range (1985–2018) is 10.1–12.5 (U.S. Environmental Protection Agency, Chesapeake Bay Program 2019).

Tidal marsh construction followed dredged material placement over shallow CB bottom within containment cells, surrounded by sand perimeter dikes approximately 3 m in height above mean sea level (MSL). The substrate was fine-grained dredged material (Cornwell et al. 2020) to a depth of approximately 2 m, after consolidation. The tidal exchange was established via inlets through the external dike approximately six months before planting. The marshes, ranging in size from approximately 12 to 20 ha, were designed with elevations to provide 80% LM, planted with *S. alterniflora*, and 20% HM, planted with *S. patens* (U.S. Army Corps of Engineers 1996). The completed Poplar Island (PI) marshes were constructed sequentially over 15 years, providing marshes ranging in age from approximately 3–18 years for this study.

Marsh Elevation

Marsh elevation was measured annually using deep-rod Surface Elevation Tables (SETs) (Cahoon et al. 2002a, b; Callaway et al. 2013). Measurements began in Cells 3D and 1A in 2009 and were made annually through 2022 in late winter or early spring before the onset of vegetation growth (Staver et al. 2020). Other sites were added as new cells were developed. Marker horizon data were not available.

Data presented here include the least-squares regression slope of elevations recorded in each of the four compass directions at every SET. Rates of elevation change were compared to the recent SLR trend at the Annapolis, Maryland tide gauge (NOAA Station 8575512) calculated from monthly mean sea level data for years 1995 through 2022.

We fitted a linear model (SAS© 9.4 Proc Reg) to the SET data to calculate the slope for each time series. The data set included all SET plots in all wetland cells except the newly developed Cell 5AB. No attempt was made to clean the data, and in each case, the entire time series was used in the calculation regardless of abrupt changes in slope as determined by visual inspection of the data or premature termination of the data record. In addition, there was no averaging of the time series data from individual SET subplots. Slopes were computed for the individual time series recorded at each SET compass direction.

Above- and Belowground Biomass

Annual macrophyte production was estimated by harvesting aboveground (AG) and belowground (BG) biomass samples in September or October. Six HM and at least six LM sites scattered throughout each marsh to maximize spatial coverage were sampled each year beginning in 2009. Before 2009, sampling did not occur at the same locations and did not always include BG sampling. AG biomass samples were harvested using 0.25 m^2 quadrats and separated into dead and living biomass before being dried at 60 °C for a minimum of three days in a forced draft oven and weighed. BG biomass samples consisted of a single sediment core collected from within each of the AG biomass quadrats using a specially fabricated 7.3 cm diameter stainless steel piston corer. Sediment cores were washed free of sediment over a 1 mm mesh sieve before being dried and weighed. The reported measurements are composites of live and dead BG biomass. The root-to-shoot ratio (RSR), which includes rhizomes, was calculated as the ratio between BG and AG_{Live} biomass.

Sediment Cores

Sediment cores collected with a 7.3 × 25 cm stainless steel piston corer as part of annual biomass sampling in 2010 were used to determine the vertical distribution of *S. alterniflora* BG biomass. Core depth was not uniform, but cores were sliced into 2 cm disks, and each disk was hand-sieved with running water over a 1 mm mesh nylon sieve to remove sediment. To characterize the BG biomass distribution of *S. patens*, HM soil cores were obtained in 2021 and processed similarly, except that each disk was cleaned in a Gillison's

hydropneumatic root washer before hand-sieving. In each case, roots and rhizomes were not separated, and all root/rhizome material was dried at 60 °C to constant weight in a forced draft oven as described above. Additional analyses included soil macro-organic matter (MOM), determined by loss on ignition (LOI). Sediment samples collected in 2021 were ashed at 500 °C for 4 h to determine LOI (Dean and Walter 1974).

The Coastal Wetland Equilibrium Model (CWEM)

The Coastal Wetland Equilibrium Model (CWEM v.10.8), formerly the Marsh Equilibrium Model (MEM), has been modified for this application with the addition of a revised front end and an option to simulate marsh development. MEM has been described elsewhere in detail (Morris et al. 2021; Morris and Callaway 2018; Morris and Sundberg 2024). CWEM features a revised model of sediment diagenesis referred to as a cohort model. The cohorts are dynamic; their composition and volumes vary with the depth of the cohort due to the turnover and decomposition of roots and rhizomes. The model front end refers to how the sediment cohorts are initialized.

Conceptually, a wetland pedon can be considered to be a stack of annual laminations or cohorts that are buried by successive generations of cohorts (Morris and Bowden 1986). The top and newest cohort is formed from a deposit of minerals and organic matter settling out from that suspended in flood and tidewater or litterfall. The organic deposition was discounted in this implementation of CWEM. We assumed that storms and tides remove the litter and that suspended organic matter is entirely labile. At ever greater depths, the cohorts are invaded by live roots and their decay products, which add volume. Eventually, below the root zone, the volume may decrease temporarily as the added organic matter stabilizes and labile organic matter decays. The final cohort volume consists of the original sediment deposit plus the total production of refractory organic matter in the layers above.

As described elsewhere (Morris et al. 2022), the model was started by populating the cohorts with initial quantities of organic and inorganic matter. We used empirical LOI profiles in conjunction with the ideal mixing model to populate the cohorts. By equating cohort volume (cm^3) to the annual rate of vertical accretion (dZ/dt) per cm^2, and from a known dry LOI (g/g), it is possible to compute the weight and volume of both the organic and mineral fractions from the ideal mixing model: $BD = 1/[LOI/k_1 + (1 - LOI)/k_2)]$, where k_1 and k_2 are the self-packing densities of organic and mineral matter, LOI is the loss on ignition (g/g), and BD is dry bulk density (g/cm^3) (Morris et al. 2016). The volume of a cohort, which in equilibrium is equivalent to the rate of vertical gain, is $V_T = V_o + V_i$; then, $V_T = W_o/k_1 + W_i/k_2$, where V_o, W_o, V_i, and W_i are the volumes and weights of organic and mineral matter, respectively. Thus, every cohort can be populated with organic and mineral weights from the profile of LOI. However, the fractionation of organic matter between labile and refractory parts is unknown, except below the root zone where all or a majority of W_o is refractory. We assumed that the initial labile fraction was zero because it has a fast decay rate. The live root fraction was empirically derived from sediment cores taken from the restoration sites. After subtracting the live fraction from W_o, the remainder was assumed to be refractory.

Vertical accretion in a saltmarsh largely depends on the production of biovolume which is strongly affected by relative elevation (Morris et al. 2012; Morris and Sundberg 2024; Owers et al. 2022). Where there is little or no accumulation of surface litter, new biovolume is generated from the turnover of BG biomass. New biovolume is the refractory portion of that turnover, and this is proportional to the standing biomass, which is a function of relative elevation. McKee and Patrick (1988) showed that *S. alterniflora* has a vertical growth range that spans a distance a bit greater than the tidal amplitude, centered approximately between MSL and the mean high water (MHW) level. For several species examined, including *Spartina alterniflora*, growth at the high end of the vertical growth range is constrained by osmotic stress (salinity and drought), while at the low end of the range, growth is constrained by hypoxia (Mendelssohn and Morris 2000). A field bioassay experiment (marsh organ) showed that *S. alterniflora* at North Inlet, SC grows between approximately 10 cm below MSL and about 30 cm above MHW with an optimum for productivity and standing biomass in the middle of the range (Morris and Sundberg 2024; Morris et al. 2013b). This seems to be a good rule of thumb that extends to estuaries differing in tidal range. We can describe the vertical biomass (B_s) profile generally as a function of relative elevation (Z) as:

$$B_s = a\,(\text{MHW-Z}) + b\,(\text{MHW-Z})^2 + c \quad (1)$$

But with two species, two equations define their distribution (Morris 2006). Moreover, if the distribution is asymmetrical as we assume here, there are two equations for each species—one for the left half of the curve and one for the right side. And, for a marsh restoration or creation as on Poplar Island, this curve changes significantly as the marsh community matures. Craft et al. (2002) estimated *Spartina cynosuroides* standing biomass required 9 years to fully develop, while *S. patens* was not fully developed after 15 years. Soil macro-organic matter generally developed at rates like AG biomass. Consequently, it was necessary to describe how the vertical growth range, its optimum depth, and maximum biomass vary with age. We assumed for simplicity that growth is linear to the point of maturity. Hence, for restoration, there are growth factors defined, for example, as

$$\mathrm{GF}_{B\max} = \left(B_{\max\,(\mathrm{mat})} - B_{\max\,(0)}\right)/T_{\mathrm{mat}} \quad (2)$$

where $B_{\max(0)}$ and $B_{\max(\mathrm{mat})}$ are the maximum standing biomass of young and mature marsh, respectively, and T_{mat} is the time to maturity (years). These growth factors were computed for maximum standing biomass, and root turnover rate. For both species, Eqs. 1 and 2 were updated annually using the growth factors to compute the updated variables $B_{\max}$ and so on until time T_{mat}.

On Poplar Island, the vertical distributions of *S. alterniflora* and *S. patens* overlap, which implies that the boundary may be determined by competition between the two species. There are different models of density-dependent plant competition based on what is referred to as empirical replacement series experiments (Park et al. 2003). Bertness (1991) described the competition between *S. patens* and *S. alterniflora* as a physical limitation of *S. patens* at the low end of its fundamental (*sensu* Hutchinson (1957)) distribution and competition from *S. patens* as excluding *S. alterniflora* at the high end of the gradient. What we observe on Poplar Island are patchy distributions where the species overlap, with *S. patens* growing on tussocks. We have used a "winner take all" rule to model the outcome of competition between these species. Where the distributions overlap at a declining stage of the prior community and early stage of the succeeding plant community, whichever species has the greater biomass at a given elevation prevails. As the standing biomass of a community decreases, i.e., on the suboptimal side of the vertical growth distribution, the living root biomass also decreases. The model accounts for this decrease as mortality, divided between labile and refractory organic matter. The labile pool decays, and this may decrease the volume of cohorts (and elevation), while the refractory pool is permanent. Currently, the mortality of roots that would occur at the transition to the successor species is unaccounted for. This will cause a small error in metrics of carbon sequestration and elevation change in simulations where species transitions occur.

After calculating the maximum standing biomass B_S (g/cm^2), the sequestration of organic matter is

$$\frac{dz}{dt}_{\mathrm{org}} = \frac{k_r \xi \delta B_S}{k_1} \quad (3)$$

Constants in the model are the refractory fraction k_r (g/g), the root-shoot ratio ξ (g/g), the turnover rate of belowground biomass δ (year^{-1}), and the self-packing density k_1 (g/cm^3). This simplifies to

$$\frac{dz}{dt}_{\mathrm{org}} = X_1 \delta B_s = X_1 \delta f_1(D) \quad (4)$$

where $f_1(D)$ is Eq. 1, δ is the turnover rate, and $X_1 = k_r \xi / k_1$. For the refractory fraction k_r, we use a value of 0.1 based on the lignin fraction (Buth and Voesenek 1987; Hodson et al. 1984; Morris and Sundberg 2024; Wilson et al. 1986).

The inorganic sedimentation is given by

$$\frac{dz}{dt}_{\mathrm{inorg}} = \frac{0.5 q m f D \tau}{k_2} \quad (5)$$

Parameters are the dimensionless capture coefficient q, the concentration of suspended inorganic matter m (g/cm^3), flood frequency f (year^{-1}), depth D below MHW (cm), fractional inundation time ($0 \le \tau \le 1$), and self-packing density k_2 (g/cm^3), respectively. The coefficient 0.5 is used to approximate a square wave. This simplifies to

$$dz \Big/ dt_{\mathrm{inorg}} = q f_2 D$$

where

$$f_2 = \frac{0.5 m f \tau}{k_2}. \quad (6)$$

Finally, a static version of this model was fitted to the measured accretion rates by multiple linear regression:

$$dz \Big/ dt = X_1 \delta f_1(D) + q f_2(D) \quad (7)$$

Depth D was taken from the mean elevation of each SET time series, and dz/dt was the regression slope (accretion rate). Equation 7 was fitted to the entire collection of empirical rates of elevation change, and the regression coefficient was the estimated turnover rate δ. Parameter values are given in Table S1.

Simulated Permutations

A variation of the model was run to demonstrate the effect of marsh development. The SET elevations were averaged over the entire group of LM SET platforms, after removing outlying 2010 and 2020 means and excluding Cell 5AB. The total number of observations each year varied from 540 to 846. Hindcasts were run by starting the MSL at 6.1 cm NAVD88 (Fig. 1) and marsh elevations to the 2009 SET elevations (cm NAVD88), 24.4 ± 0.22 cm for LM and 63.89 ± 1.23 cm for HM. The default was a simulation that allowed for marsh development and expansion of BG biomass. The AG standing biomass at the start was 279 g/m^2 at a relative elevation of 18.4 cm, an RSR (ξ) starting at 2 and ending at 1.5 at maturity, and a starting turnover rate (δ) of 1/year, declining to 0.5/year at maturity. Other model parameters were held constant. For comparison, a simulation of a fully developed marsh was run, starting at the same elevation and biomass of 1926 g/m^2, an RSR of 1.5, and a turnover time of 0.5. Other numerical experiments included permutations of starting elevation (LM and

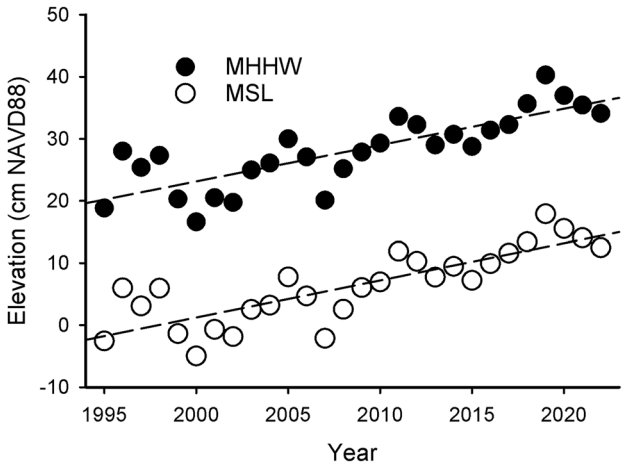


Fig. 1 Mean sea level (cm NAVD88) recorded at the Annapolis, MD gauge (NOAA Station ID: 8575512), computed from monthly means. The regression slope is 0.57 cm/year ($R^2 = 0.63$, $P < 0.0001$)

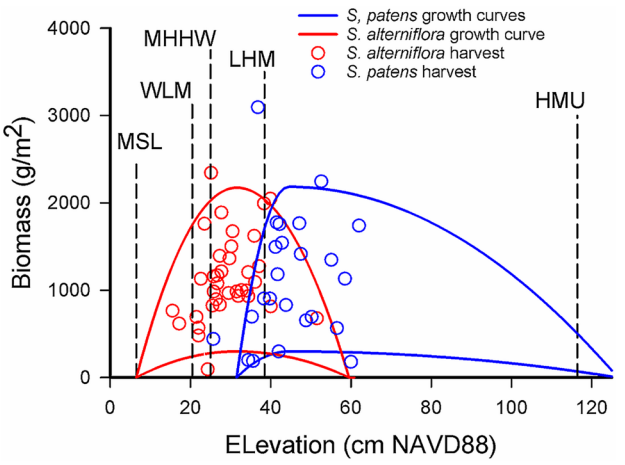


Fig. 2 Tidal datums, community boundaries, growth range, and observed standing biomass. Community boundaries divide open water from low marsh (WLM at 20.5 cm NAVD88), low marsh from high marsh (LHM at 38.4 cm NAVD), and upper high marsh (HMU at 116.6 cm NAVD88) from a terrestrial community. The tidal datums are the current mean sea level (MSL) and mean higher high water (MHHW) level from the regressions in Fig. 1. These various datums inform the assumed growth limits of early-stage and late-stage *S. patens* (——) and *S. alterniflora* (——). Aboveground harvest data are shown in Table S2

HM), rate of sea-level rise (RSLR), and a simulation of thin layer placement (TLP); all allowed for marsh development.

The Static Fit of the Coastal Wetland Equilibrium Model (CWEM)

As a test of internal consistency, a simplified version of the CWEM model, Eq. 7, was fitted using nonlinear regression (SAS© v 9.4 Proc Model) to mean SET elevation change binned by elevation. Vertical change, *dZ/dt* (the dependent variable), was first computed from the slope of each linear time-series regression and the mean rates were computed in bins of 4 cm of surface elevation. Surface elevation was the independent variable and was computed in each bin as the average of the relative elevations of each SET time series. Standing biomass was computed for each bin from Eq. 1. The turnover rate coefficient δ in Eq. 4 was treated as an unknown. The other term in the model was the vertical sequestration rate of inorganic matter, Eq. 6, where the capture coefficient q was treated alternately as a known and an unknown. Other coefficients were known with varying degrees of certainty. Parameters in Eq. 6, such as inundation time, were calculated from known observations. Negative elevation changes were entered as zeros when fitting the model.

Results

Mean Sea Level and Trend

The recent sea-level trend in Annapolis from 1996 to 2021 was 5.7 mm year^{-1} (Fig. 1). This rate exceeds the global mean sea level trend of 3.6 mm year^{-1} over the period 2006–2015 (Oppenheimer et al. 2019). The elevated rate of SLR in the mid-CB and environs is a result of regional isostatic change combined with the withdrawal of groundwater leading to subsidence rates of 1.5 to 3.7 mm year^{-1} (Davis 1987; Eggleston and Pope 2013). The 2009 intercept of 6.06 cm NAVD88 (Fig. 1) was accepted as the starting MSL of Poplar Island simulations.

Datums and Standing Biomass

The growth ranges of *S. alterniflora* and *S. patens* were constructed based on boundary surveys and plant harvest data (Fig. 2). The biomass harvests at surveyed elevations document that the two *Spartina* spp. occupy overlapping vertical ranges. The average present-day boundary in Cell 1A between vegetated, low marsh habitat and mudflat lies at an elevation of 20.5 ± 5.1 cm NAVD88 (± 1 SD) (Fig. 2). The average boundary between low marsh, *S. alterniflora* habitat and high marsh, *S. patens* habitat is 38.4 ± 3.1 cm, which is close to the present-day, mean higher high water (MHHW) level of 34.9 cm NAVD88. The vertical growth range varies among estuaries with tide range, and the empirical range here is consistent with the known vertical range of *S. alterniflora* in other estuaries (Morris et al. 2013b). Moreover, the empirical range (LHM-WLM) of 18 cm is close to the tidal amplitude of 21.8 cm. The average elevation of the upper boundary of the *S. patens* community was 116.6 ± 19.8 cm NAVD88. The average AG biomass density

of harvests from the Cells 1A-1C *S. alterniflora* community was 1227 ± 344 g m^{-2} (n = 14). The mean of surveyed elevations (2021) in low marsh locations was 31 ± 4 cm NAVD88 (n = 20), while the average biomass density of *S. patens* was 1722 ± 868 g m^{-2} (± 1 STD, n = 11). The average of surveyed high marsh elevations was 50 ± 8 cm NAVD88 (n = 16). The lower curve of each species (Fig. 2) is the presumptive biomass distribution after planting—the early stage. The higher curve of each pair shows the presumed distribution of the mature or late-stage marsh community.

Observed Elevation Change and the Static Model

A least-squares fit of the static version of CWEM (Eq. 7) returned a turnover coefficient δ of 1.4 ± 0.14 $year^{-1}$ (P < 0.0001) irrespective of the treatment of the capture coefficient as a known or unknown. The best-fit value of δ is close to the value used for young, early-stage marshes (Table S1) and consistent with theoretical arguments about allometric ratios (Morris et al. 2013a) and empirical data (Morris and Sundberg 2024). When treated as an unknown, the best-fit value of q was 0.35 ± 1.9 $year^{-1}$ (P = 0.86) and the overall model R^2 was 0.44. When q was entered into the model with a known value of 2.8 (Morris and Sundberg 2024), the model R^2 was 0.42 (RMSE = 0.22). Inorganic inputs are small relative to the rate of organic sequestration (Staver et al. 2020), which accounts for the insensitivity of the model to q and its statistical insignificance when treated as an unknown.

The trend in marsh elevation change (Fig. 3) paralleled the predicted growth curve of marsh vegetation (Fig. 2). The high points between 20 and 30 cm relative elevation corresponded to the modeled elevation optima for biomass as well as the maximum observed biomass. The maximum observed rates, 0.97 ± 0.08 (± 1 SE) and 0.87 ± 0.03 cm/year at 22 to 26 and 26 to 30 cm rel MSL, were greater than the maximum model calculated rate of 0.6 cm/year, but the trends were qualitatively consistent. Both observed and modeled elevation change decreased at higher elevations. The observed elevation change was also lower at lower relative elevation. But as the elevation of the marsh rises relative to sea level, the frequency and duration of inundation and the rate of sediment accumulation are diminished (Krone 1987). Conversely, as relative elevation falls, mineral sedimentation becomes more important and eventually dominates as the depth of flooding D increases (Eq. 5). The observed and modeled trends at elevations between 10 and 30 cm (Fig. 3) are opposite what the trend in mineral sedimentation should be and demonstrate the importance of organic accretion. Below the lower limit of vegetation, i.e., elevations less than MSL, the modeled elevation change increased with increasingly negative elevations due to mineral sedimentation.

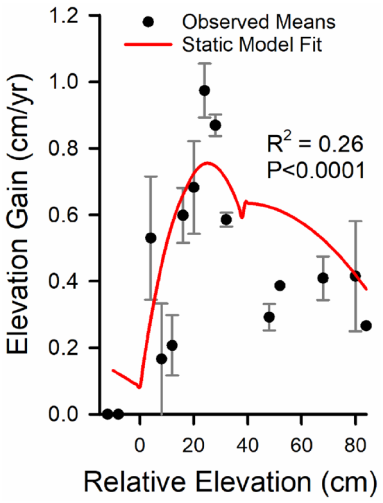


Fig. 3 Shown are the observed rates (•) of elevation change (± 1 SE) in 4 cm elevation bins and rates computed from a static model (Eq. 7) fit plotted against relative (to MSL) elevation. The model was fitted to the binned means with known q = 0.28

Low and High Marsh Elevation Change

The starting, mean elevation of LM SET sites had observed and simulated elevation change of 0.51 ± 0.04 cm/year and 0.41 cm/year, respectively (Fig. 4A). LM was defined as having an elevation (Z): 20.5 ≤ Z ≤ 38.4 cm NAVD ($\overline{Z}$ = 24.4 cm, n = 189). The detail in Fig. 4A shows that the simulated elevations fitted the observed data exceptionally well through the first decade.

Elevation change recorded at the HM SET platforms was lower than LM SETs. Observed and simulated rates were 0.36 ± 0.03 cm/year, n = 14, and 0.37 cm/year (Fig. 4B), respectively. HM was defined as having an elevation: Z > 38.4 cm NAVD ($\overline{Z}$ = 63.9 cm, n = 108), and the simulation was started at the mean of the time-zero HM marsh elevations. In the constant, 0.57 cm/year SLR simulation, the HM was predicted to transition to LM by the end of the century. In the centenary sea-level rise (CSLR) to 100 cm simulation, the HM was predicted to transition to LM by 2060 and to drown by 2085 (Fig. 4C).

Marsh Survival Time

The simulation of LM at constant SLR (Fig. 4B) shows that the predicted NAVD elevation will begin to decrease starting about 2030, and by 2050 (43 years from the start), the marsh will drown. The survival time decreased with an increase in the rate of SLR. This was shown by the 100 cm CSLR scenario which advanced the loss of LM to the year 2030. Survival time increased by raising the elevation to the range of HM vegetation, 63 cm NAVD. At a constant SLR of 0.57 cm/year, the HM marsh survived a century

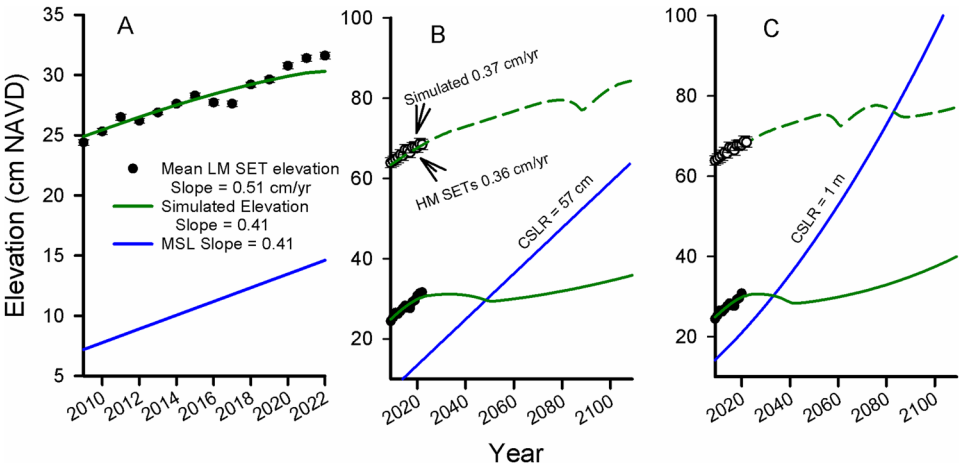


Fig. 4 Time series of observed SET elevations (o), simulated elevations (—), and sea level forecasts (—). The first 15 years are shown in **A** for an LM simulation in which the RSLR was held constant at the current rate, 0.57 cm/year, while in **B**, the 100-year simulation at constant SLR is shown for LM (—) and HM (— —) simulations with the mean SET elevations. Shown in **C** are the simulated and observed LM and HM elevations resulting from an acceleration in SLR, rising to 100 cm in a century (—)

but transitioned to low marsh. The LM marsh was lost after 75 years in the 100 cm CLSR scenario.

Simulated Low Marsh Biomass

The initially high vertical elevation gain of the LM and its early demise is best explained by (1) its vegetative growth during the first stages of the development and (2) its relatively low initial elevation (Fig. 5). With a starting elevation lower than the optimum, an increase in the RSLR will decrease biomass, and decrease relative elevation, leading eventually to a drowned marsh. However, the LM was almost keeping up with sea-level rise today by virtue of a growth premium. As the marsh matured, it added volume to the soil from the increase in biomass and turnover of living roots and rhizomes. After the marsh matures, only the turnover of roots and rhizomes adds volume. While the growth premium was able to maintain relative elevation in approximate stasis, after maturity, the added volume slowed, and the marsh, which then was on the suboptimal side of its vertical growth distribution, began to lose relative elevation (Fig. 5).

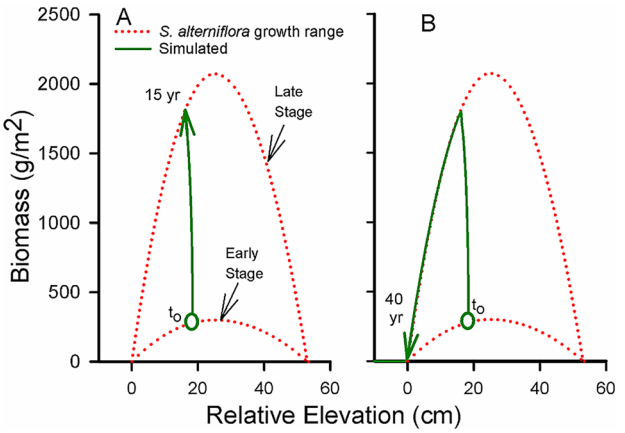


Fig. 5 Assumed biomass profiles of early and late-stage *S. alterniflora* (.....) and predicted biomass trajectories (—). In **A**, the biomass trajectory is shown during the first 15 years, and in **B**, the 100-year biomass trajectory is shown. The current rate of SLR, 0.57 cm/year was held constant. The initial marsh elevation was set at 18.6 cm rel MSL

Simulated High Marsh Biomass

The dynamics of biomass in the HM simulations were complicated by the overlapping ranges of the growth curves for *S. alterniflora* and *S. patens* and a transition from HM to LM (Fig. 6). The green lines are biomass time series plotted against elevation. The simulations were started at a relative elevation that is solely within the modeled growth range of *S. patens*. The development of this marsh was almost able to maintain a constant relative elevation, but after maturity, like the LM simulation (Fig. 5), the relative elevation of the HM started to decline. In two permutations of rising sea level, one held to a constant rate, 0.57 cm/year (Fig. 6A, B), and one allowed to accelerate to 100 cm in a century (Fig. 6C), the biomass increased as the marsh matured. In both cases, the maximum biomass in the *S. patens* community reached a limit in year 25 at an AG biomass of 2,090 g/m^2 (Fig. 6B). After reaching maturity, as the gain in elevation slowed, SLR was faster than the elevation gain, and relative elevation declined.

We assumed that the transition from HM to LM would occur after rising sea level reduced the biomass and health of *S. patens* to a point where a developing *S. alterniflora* community could replace it in a winner-take-all scenario. After the transition, the biomass of *S. alterniflora* then increased as it developed (Fig. 6C). In the case of the constant 0.57 cm/year SLR scenario, the simulation ended with a fully developed *S. alterniflora* marsh at peak biomass (Fig. 6B). But, in the 100 cm CSLR scenario, rising sea level near the end of the century overtopped the *S. alterniflora* marsh.

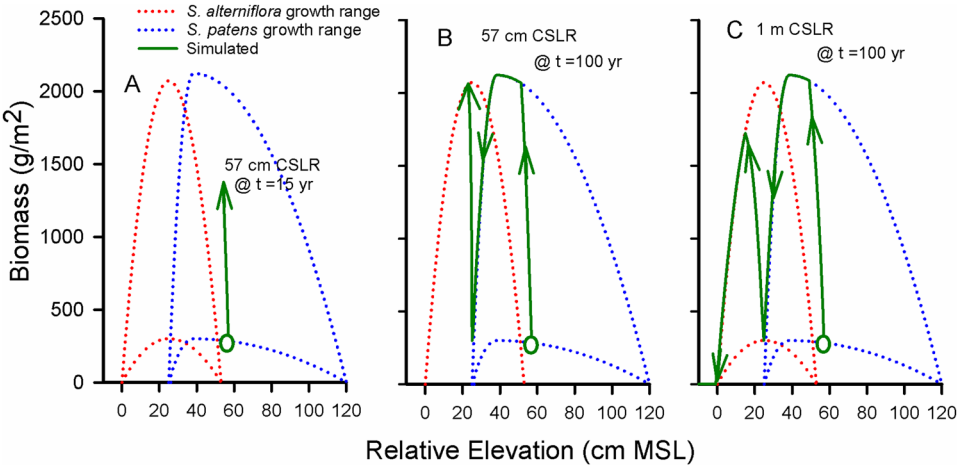


Fig. 6 Assumed biomass profiles of early and late-stage *S. alterniflora* (.....) and *patens* (.....) communities, and predicted biomass trajectories (——) started at 64 cm NAVD. The growth in biomass during the first 15 years (**A**) and 100 years (**B**) are shown when the rate of SLR was held constant at 0.57 cm/year and (**C**) when projected to rise 100 cm in a century (CLSR). The initial marsh elevation was 57.8 cm relative to 2009 MSL

Simulated LM and HM Sediment Organic Matter Profiles

The simulated developmental history of the marshes is recorded in their sediment organic matter profiles (Fig. 7). For example, a secondary peak LOI found in the LM at 12.8 cm was predicted to move in 15 years to a depth of 18.1 cm below the surface (Fig. 7A). This gives an elevation gain of 0.35 cm/year compared to the simulated SET gain of 0.41 cm/year (Fig. 4A). After 100 years, the secondary peak had moved to 23.9 cm which gives a gain of 0.1 cm/year. The decline was due to the loss of vegetation. Using the same starting LOI profile for HM, the secondary LOI peak moved from 12.4 to 17.9 cm in 15 years (Fig. 7C), which gives an accretion rate of 0.36 cm/year compared to a simulated SET gain of 0.37 cm/year. After 100 years, the HM secondary peak had moved to 34 cm, which gives an elevation gain of 0.22 cm/year. These secondary LOI peaks are analogous to geochronological markers such as peak ^{137}Cs. The discrepancies between the calculations of elevation gain using the proxy geochronologies at 15 years, e.g., 0.35 cm/year vs. 0.41 cm/year (Figs. 7a and 4A), are affected by the shrinking of sediment cohorts as they lose root biomass and labile necromass while they transit through the sediment.

In general, the sediment LOI of a marsh will increase over time as relative marsh elevation rises. In both HM and LM, the LOI concentrations were predicted to increase during the first 15 years, during the growth phase (Fig. 8A, C). During the growth phase, the peak LOI was near the surface

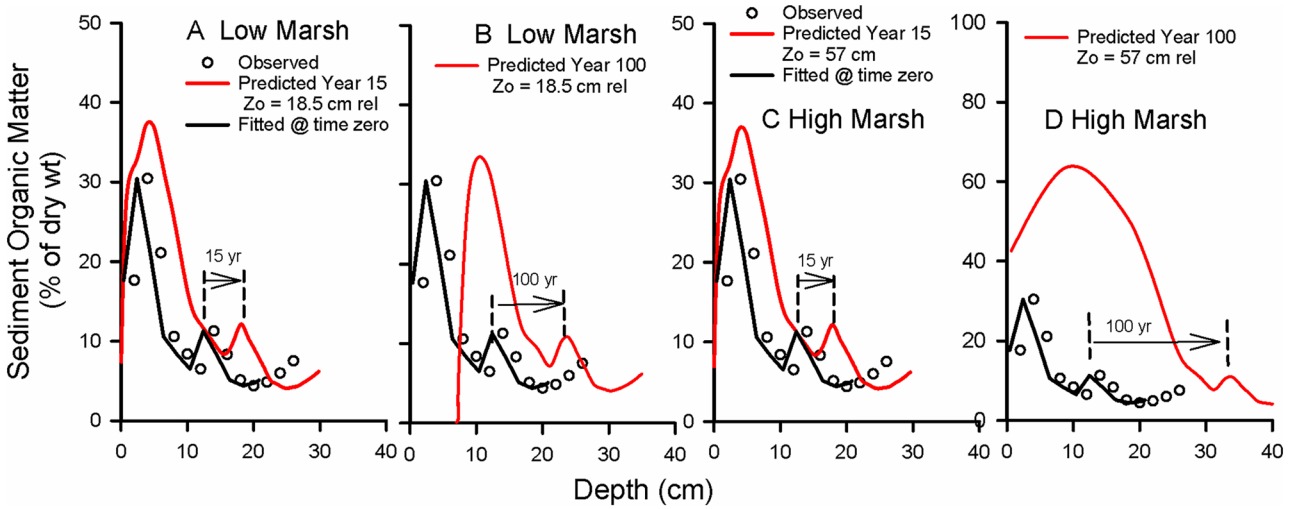


Fig. 7 Observed and predicted depth profiles of sediment organic matter. The model sediment cohorts were populated at t_0 with observed (—o—) depth profiles of sediment organic matter concentration (LOI) from the HM. The LOI depth profiles evolve and appear after the first 15 years of simulation as (——) in **A** and **C** and after 100 years as in **B** and **D**. The initial elevation was 16.4 cm relative to 2008 MSL, and in **C** and **D**, initial elevation was 57.8 cm rel MSL. SLR was held constant at the current rate of 0.57 cm/year

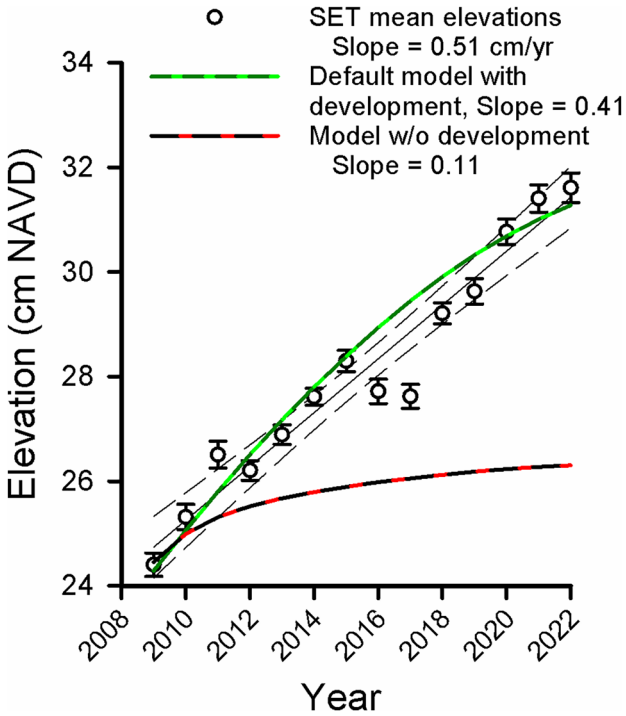


Fig. 8 Model simulations of marsh elevation with and without development. Shown are the mean elevations (±1 SE) of all LM plots, and the simulated elevations of a developing marsh (—) and a mature marsh (—)

where the greatest concentrations of roots occur (Fig. 8A, C), but as the relative elevation of a marsh decreased, the input of sediment increased, diluting the LOI near the surface. As the simulations proceeded, new cohorts were added to the surface and the volumes and compositions of existing cohorts were changed by the growth, turnover, and decay of roots and rhizomes. In the LM simulation, after the marsh drowned, the only input to the marsh surface was mineral, and this is seen in the LOI profile where the LOI dropped to zero in the top 15 cm (Fig. 7B). The HM survived 100 years, and its LOI increased to the highest level, about 60%, by the end-of-simulation (EOS) (Fig. 7D).

The LM Simulation with and Without Marsh Development

CWEM was run with and without marsh development to illustrate the growth premium effect. When the model was started with parameters that characterize a fully developed marsh, the 15-year elevation gain was 0.11 cm/year (Fig. 8). The early rise in elevation in this simulation is from the model equilibrating the elevation to the starting conditions imposed on the model. In other words, the starting elevation was less than what the parameter values dictated. When started at an early developmental stage, the simulated accretion rate was 0.3 cm/year greater.

Simulated LM Thin Layer Placement (TLP)

The do-nothing scenarios are not sustainable at the current or higher rate of SLR. The LM was predicted to drown in about 33 years when the rate of SLR was assumed to accelerate to a level of 100 cm (Fig. 4B). Simulations demonstrate that TLP can be a successful method of extending marsh survival (Fig. 9). When 30 cm of sediment (compacted depth) was added to the surface starting in year 30 and repeated at 30-year intervals, the marsh was able to track MSL in steps (Fig. 9A). This simulation assumed also that each application of sediment returned the marsh to an early stage of development (Fig. 9C). Consequently, a cycle of marsh development was established with the additional advantage that repeated cycles of rapid growth of BG biomass should raise long-term elevation gains as seen in the early stage of the LM simulation (Fig. 4A). The episodic pulses of sediment resulted in episodic changes in elevation (Fig. 9A) and biomass (Fig. 9B). Biomass will increase during the growth phase and decline as sea level overtakes the marsh; then, a pulse of sediment will raise the elevation and a new growth phase will begin. The elevation was predicted to move back and forth between the HM and LM, resulting in a complex pattern of community dynamics (Fig. 9C).

Carbon Sequestration

The configuration and management of the marshes have a significant effect on carbon sequestration and inventories. The integrated rate of carbon sequestration (RCS), computed as $\mathrm{RCS} = ck_r\xi\delta \sum_{t=1}^{100} B_S(t)$, varied from a low of 17 to a high of 78 g C m^{-2} $year^{-1}$, depending on the conditions (Table 1). Here, c is the conversion factor (0.55) or quotient of elemental carbon to total dry organic weight (Drexler et al. 2009). In most cases, RCS was greater at low CSLR than at higher CSLR and greater with TLP than without. However, the highest RCS, 78 g C m^{-2} $year^{-1}$, resulted from a combination of high starting relative elevation, 57 cm CLSR, and no TLP applications. TLP applications at low SLR and high elevation resulted in elevations that were superoptimal. At low CSLR and low elevation, the highest RCS, 72 g C m^{-2} $year^{-1}$, resulted from three TLP applications per century of 15 cm each (Table 1). At high CLSR and low elevation, the highest RCS, 62 g C m^{-2} $year^{-1}$, was seen when 30 cm of TLP was applied three times.

The total EOS carbon inventory was computed as the total standing stock of organic carbon (live and dead) after a century, including the starting pool of refractory carbon. The greatest carbon inventory, 18 kg C m^{-2}, and volume of soil organic matter (SOM), 38 cm^3/cm^2, were obtained in an HM simulation without TLP at a CSLR of 57 cm (Table 1). The smallest volume of SOM, 20 cm^3/cm^2, and C-inventory, 9 kg C m^{-2}, were found when the simulation was started without

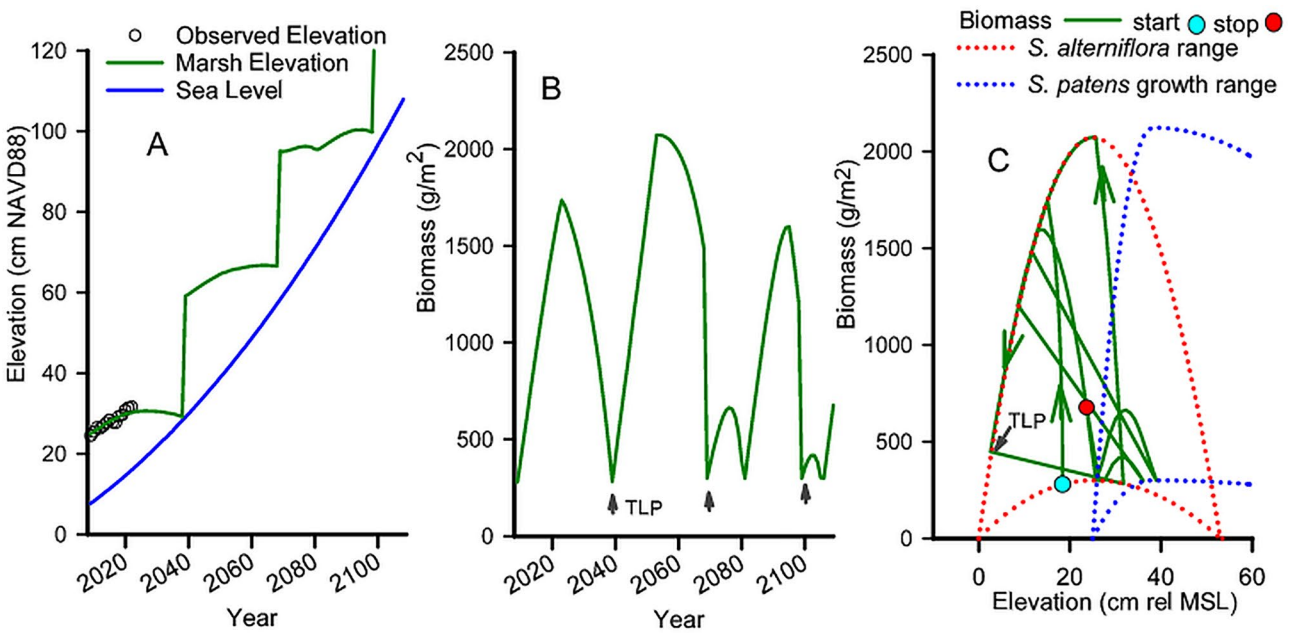


Fig. 9 Simulation results of thin layer placement (TLP). Results of simulated TLPs of 30 cm in years 30, 60, and 90 shown in **A** are the observed elevations (o), MSL rising to 100 cm NAVD in a century (—), and the predicted marsh elevation (—). The predicted standing biomass is shown in **B**. In **C**, biomass is plotted against relative elevation. Also in **C** are the early and late growth ranges of *S. alterniflora* (.....) and *S. patens* (.....)

Table 1 Numerical tests computed over two centenary sea-level rise (CSLR) scenarios showing end-of-simulation (EOS) results of different TLP applications: none or starting 30 years from the start and repeated 3 or 5 times at 15 or 30-year intervals during the century and applied depths of 15 or 30 cm

CSLR	TLP applications (cm)	Starting Elevation (cm rel MSL)	EOS marsh elevation (cm NAVD)	EOS SOM volume (cm^3/cm^2)	EOS C inventory (kg C m^{-2})	Sequestration rate (RCS) (g C m^{-2} $year^{-1}$)	Survive to year 100
57 cm	None	18.5	36	21	10	22	No
	3×15=45 cm	18.5	89	36	17	72	Yes
	5×15=75	18.5	118	34	16	70	Yes[b]
	3×30=90	18.5	132	33	16	66	Yes[b]
	None	57.8	85	38	18	78	Yes[a]
	3×15=45	57.8	128	35	17	76	Yes
	5×15=75	57.8	154	32	15	63	Yes
	3×30=90	57.8	168	31	14	62	Yes
100 cm	None	18.5	40	20	9	17	No
	3×15=45 cm	18.5	80	22	10	27	No
	5×15=75	18.5	115	32	15	60	Yes
	3×30=90	18.5	130	32	15	62	Yes
	None	57.8	78	28	13	55	No
	3×15=45	57.8	129	37	17	75	Yes[a]
	5×15=75	57.8	157	35	16	71	Yes
	3×30=90	57.8	172	35	16	74	Yes

All simulations started at 6.5 cm NAVD sea level and a relative marsh elevation of 18.5 or 57.8 cm. The measured LOI profile (see Fig. 7) was used to populate time-zero cohorts, which numbered 60. Soil organic matter initially occupied 17.3 cm of vertical space over a total sediment depth of 24.8 cm and contained 7.7 kg C m^{-2}

[a]HM transitions to LM

[b]LM transitions to HM

TLP in LM at the higher CSLR. With TLP, the greatest inventory and SOM volume, 17 kg C m^{-2} and 37 cm^3/cm^2, were found in the HM simulation at three TLP applications of 15 cm each. The RCS and EOS carbon inventory were highly correlated, $R^2 = 0.98$: RCS (g C m^{-2} $year^{-1}$) = 7 EOS (kg C m^{-2}) – 43.

Discussion

Thin layer placement or TLP of sediment onto the marsh at periodic intervals can be a successful strategy for increasing marsh resilience to rising sea level. Numerical experiments with none or 3 different TLP strategies gave different marsh responses, depending on the initial marsh elevation (HM or LM) and CSLR (Table 1). One benefit of TLP is a periodic boost in elevation, which can be fine-tuned on the fly to actual changes in sea level. A less obvious benefit is the advantage of the growth premium that affords a developing marsh additional soil volume that accompanies the growth of BG biomass. Another benefit is the added carbon sequestration that results from this growth premium.

The rate of carbon sequestration is sensitive to the schedule and amount of TLP applications (Table 1). There is an optimal TLP strategy that depends on the rate of SLR, tide range, growth characteristics of the vegetation, ecosystem service values, and dredging costs. The benefits include sustained carbon sequestration plus the other ecosystem service values of maintaining a healthy marsh. The costs are those associated with the dredging and filling operations, and the temporary loss of some ecosystem services while the marsh is recovering. The maximum rate of carbon sequestration in the LM at PI was found when the RSLR was a constant 0.57 cm/year and when three 15 cm layers were added at 30-year intervals (Table 1). However, when the CSLR was 100 cm, the maximum rate in LM was found when there were 3 applications of 30 cm each. At the current rate of SLR, the simulated HM carbon sequestration without TLP, 78 g C m^{-2} $year^{-1}$ (Table 1), is equivalent to the mean carbon sequestration rate of 79 ± 46 g C m^{-2} $year^{-1}$ found in a study of east coast estuaries (Weston et al. 2023).

A principle of marsh restoration or construction is to establish the relative elevation of the marsh on the side of negative feedback, i.e., on the superoptimal side of the growth curve (high relative elevation). The trajectory of development of a marsh will depend on the initial elevation and amplitude of the growth curve, which will vary along the development time continuum (Fig. 10A). Marsh longevity is proportional to the position of a marsh within the tidal frame, which determines its elevation capital. If the gain in elevation is less than the RSLR and relative elevation is on the side of positive feedback, the marsh may not survive, because an increase in sea level will decrease both relative elevation and biomass. It may survive if the combination of mineral deposition and growth of biovolume exceeds RSLR, moving relative elevation to the side of negative feedback, i.e., the superoptimal side for growth. If the relative elevation is on the side of negative feedback, either by design or by growth and development, and the vertical gains are less than the RSLR, then biomass and absolute elevation will rise together as relative elevation decreases until equilibrium is achieved.

A study of marsh elevation change in mature, east coast marshes using geochronological dating of sediment cores gave a mean rate of 0.3 ± 0.13 cm/year (Weston et al. 2023). The major significance of the Weston study was the finding that elevation gains have increased as the rate of SLR has risen, which can be best explained as a consequence of declining relative elevation and rising productivity. The elevations of these sites are currently high in the tidal frame and, historically, they likely were in the superoptimal range

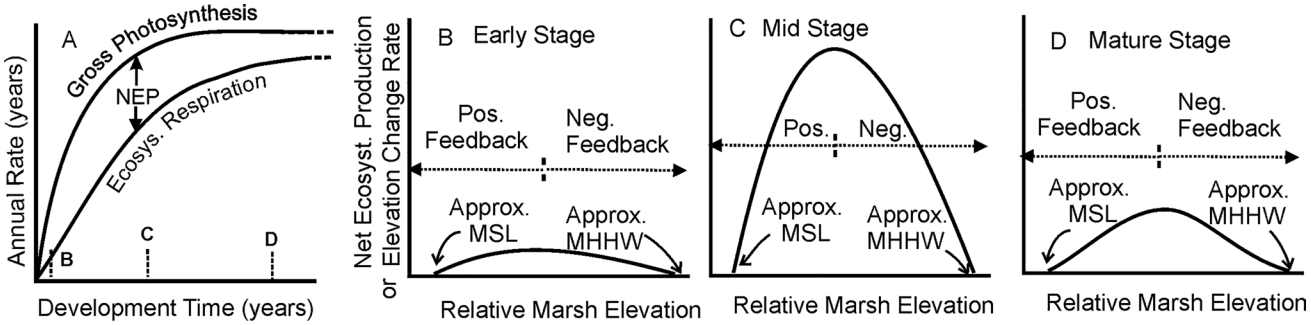


Fig. 10 Application of the theory of ecosystem development (Odum 1969) to a marsh. **A** Gross photosynthesis increases rapidly at first as biomass expands. Total ecosystem respiration lags, and net ecosystem production (NEP) reaches a maximum at mid-stage (**C**). The timing depends on the growth rate of biomass and SLR. Gross photosynthesis, limited by self-shading (Morris and Jensen 1998), reaches a plateau in mature stage (**D**). Total respiration approaches gross photosynthesis in stage (**D**), which reduces NEP. NEP is the difference between gross photosynthesis and total ecosystem respiration and in the mature stage should be proportional to the refractory fraction of production that accumulates in the sediment. At maturity, NEP fills the accommodation space and the rate of elevation change will be the lessor of NEP or the rate of increase of accommodation space

where rising RSLR would decrease relative elevation. This would increase the rates of elevation gain.

A major conclusion of the PI study is that the vertical accretion rate is greater during the early development of a marsh than in the later stages after a marsh matures. This is supported by empirical evidence (Miller et al. 2022). The observed rate of surface elevation gain at PI has been high (Staver et al. 2024) and consistent with simulations (Fig. 4). To account for these high rates, it was necessary to simulate marsh development, which allows for the growth of BG biomass. We estimate that this growth premium for *S. alterniflora* marsh is worth about 5 cm over the 15-year development time or 0.3 cm/year (Fig. 8). That is more than 50% of the current rate of vertical accretion.

The SET results at Poplar Island show that a developing marsh has higher accretion rates than a mature marsh like North Inlet, SC (Morris and Sundberg 2024), and we argue that the expansion of roots and rhizomes at PI is largely responsible for this. The evidence that BG production is substantially greater in the early stage of marsh development derives from empirical measures of vertical accretion and model results. First, consider that the average vertical accretion rate at PI in the decade or so since marshes were planted has been 5.1 mm/year (Fig. 4). At North Inlet, which has similar suspended sediment concentrations (20 mg/L), sediment composition, relative elevation, and productivity, the average vertical accretion rate of all SET platforms has been 1.9 ± 2.3 mm/year (Morris and Sundberg 2024). The LM Poplar Island simulation of late-stage marsh gave a similar vertical accretion rate of 1.1 mm/year (Fig. 7).

The constant creation of accommodation space is another factor in the development of a marsh. The sedimentary environment and rising sea level influence primary production and vegetative renewal. The production of clones from the same aging base in poor sedimentary environments is thought to lead to marsh senescence. This was demonstrated with experimental sediment additions to the surface that stimulated the formation of new shoots and buds (Fragoso and Spencer 2008). Therefore, rising sea level is beneficial to a marsh, within limits. It creates vertical space for marsh development and continuous carbon sequestration. Rising sea level will continuously raise the accommodation space.

Absent the creation of accommodation space, marsh elevation cannot increase and soil organic matter cannot grow beyond the limits of the vertical growth range. Its growth is self-limiting. In theory, the marsh could grow vertically at a rapid pace until it reaches that limit, provided that its biovolume production and mineral sedimentation exceed the rate of SLR. When the RSLR exceeds the maximum sequestration rate of organic matter and mineral deposition, the relative elevation will decrease, first at a slow rate, then more rapidly as the volume of labile organic matter decays away. Empirical observations of a rapid decrease in marsh elevation following plant mortality were explained similarly as a structural collapse of live roots (DeLaune et al. 1994).

Craft et al. (1999) found the macrophyte community on a restored North Carolina marsh matured within 5 to 10 years, but different ecosystem properties developed at different rates. The development time for a freshwater tidal marsh on the Hudson River was estimated to be < 18 years (Yellen et al. 2021). We assumed the LM biomass at Poplar Island would develop to maturity in 15 years following planting. Our simulations, supported by the SET data, show evidence of enhanced elevation gains during marsh development, a phenomenon referred to as the growth premium (Morris et al. 2023). This is a hypothesis that needs to be tested, but the logic is compelling. Macro organic matter concentration from marker horizons at PI varied with age (development time) (Staver et al. 2024), but did not cleanly increase with marsh age (Table 2). In theory, the sum of the growth of living BG biomass plus turnover in a young marsh will always exceed turnover alone.

Other variables such as sediment type and fertility are also important. Cell 4D, the oldest of the PI projects, had the lowest standing biomass (Table 2) and had a sand substrate and low nutrient concentration, which could increase the development time and the RS ratio. A field experiment at a restoration site in California examined the effects of adding different forms of nitrogen before planting, with the result that AG biomass and stem densities of cordgrass were proportional to the amount of N added (Gibson et al. 1994), which suggests that development time could be decreased and short-term vertical accretion rates increased by fertilizing restored marshes. PI and North Inlet marshes also appear to benefit from nutrient-rich sediment (Staver et al. 2024) and fertilization (Morris and Sundberg 2024). These are variables we did not consider in the present simulations with CWEM. Moreover, the RSRs in PI cells varied from 0.2 to 1.5 (Table 2), lower than we used in simulations reported here, possibly reflecting the patchy distribution of clones and mismatch in time and space between collections of cores and harvests of standing vegetation. Sediment cores and AG biomass were not collected to measure RSRs.

Table 2 Mean total belowground biomass of roots plus rhizomes to a depth of about 26 cm and mean standing live biomass from the same cells

Cell	Year constructed	*N*	Belowground biomass ± 1 SD (g/m^2)	Standing live biomass ± 1 SD (g/m^2)
4D	2003	12	1041 ± 72	680 ± 145
3D	2005	12	742 ± 46	810 ± 380
1A	2009	13	1536 ± 107	1343 ± 341
5AB	2018	10	305 ± 19	1378 ± 606

The model's assumptions that define growth and the time scales of development are critical. Unfortunately, the knowledge of the physiological determinants of the RSR, turnover, and development is limited. From a marsh organ experiment in Louisiana, Snedden et al. (2015) found RSRs of about 4:1 in *S. patens* and 2:1 in *S. alterniflora*. A 2:1 RSR in *S. alterniflora* has also been reported by Darby and Turner (2008), decreasing to about 0.5:1 in high nitrogen treatments. Merino et al. (2010) found RSRs on the order of 0.5:1. Morris et al. (2013a) argued on theoretical grounds that the RSR in *S. alterniflora* should be about 2:1. RS parameter values for young and mature marsh in the PI simulations were 2 and 1.5 for *S. alterniflora* and *S. patens*, respectively; turnover rates were 1.0 for early stage and 0.5 for the mature marsh. As used here, the RSR includes roots and rhizomes, two very different organs. The turnover of rhizomes must be relatively slow because the rhizome is a perennial storage organ (Gallagher 1983). Based on marsh organ data (Morris and Sundberg 2024), we think 0.2 year^{-1} is a reasonable turnover rate for rhizomes. In other words, a rhizome should live for about 5 years.

The functional balance theory of plant development posits that the optimal growth pattern is one in which the plant's shape convergences on a balanced growth path (Bastow Wilson 1988; Brouwer 1962; Iwasa and Roughgarden 1984), i.e., the functions of roots and leaves are balanced. Consequently, the turnover of leaves and roots must be approximately proportional, roughly 1 year^{-1}. This is consistent with the observed 1-year root longevity (Bouma et al. 2003) and with the 2–3.9 year turnover time of roots plus rhizomes of *Spartina anglica* (Hemminga et al. 1988).

There are parallels between the growth characteristics of marshes and forests. A marsh is essentially a subterranean forest with subaerial leaves. The rhizomes in a marsh are like the branches on a tree. They are long-lived, and they possess the apical meristems that grow the leaves. Rhizomes grow continuously, probably until they become crowded or until the rate of gross photosynthesis reaches a limit imposed by self-shading (Morris and Jensen 1998). Respiration will continue to increase in proportion to the total biomass like a forest (Odum 1969), eventually approaching the level of gross photosynthesis (Fig. 10A). Growth of biomass and, consequently, gains in marsh elevation should slow as respiration and gross photosynthesis approach equality. The difference between gross photosynthesis and total respiration will be the sum of sequestered, refractory organic matter plus the incremental growth of living biomass, and this sum should be proportional to the vertical change in elevation. In the late stage of development, the live BG biomass will stabilize and the elevation gains will slow. Eventually, the gain in elevation will be determined by the sequestration of refractory organic matter plus whatever mineral input exists. This leads to a hypothesis that where mineral inputs are negligible, the rate of vertical accretion is directly proportional to net ecosystem production.

Supplementary Information The online version contains supplementary material available at https://doi.org/10.1007/s12237-024-01342-x.

Acknowledgements We would especially like to acknowledge the generosity of Seth Keller (USARMY CENAB) who provided the boundary survey data.

Author Contribution James Morris: writing—original draft, review and editing, modeling, data analysis, funding, and project administration. Lorie Staver: review and editing, methodology, data acquisition, and curation.

Funding Open access funding provided by the Carolinas Consortium. This study was supported by funds from grant number 1-22-5-18-0 from the Maryland Environmental Service.

Data Availability Data for this publication is available upon request.

Open Access This article is licensed under a Creative Commons Attribution 4.0 International License, which permits use, sharing, adaptation, distribution and reproduction in any medium or format, as long as you give appropriate credit to the original author(s) and the source, provide a link to the Creative Commons licence, and indicate if changes were made. The images or other third party material in this article are included in the article's Creative Commons licence, unless indicated otherwise in a credit line to the material. If material is not included in the article's Creative Commons licence and your intended use is not permitted by statutory regulation or exceeds the permitted use, you will need to obtain permission directly from the copyright holder. To view a copy of this licence, visit http://creativecommons.org/licenses/by/4.0/.

References

Bastow Wilson, J. 1988. A review of evidence on the control of shoot: Root ratio, in relation to models. *Annals of Botany* 61: 433–449.

Bertness, M.D. 1991. Zonation of *Spartina patens* and *Spartina alterniflora* in a New England salt marsh. *Ecology* 72: 148.

Blum, L.K. 1993. *Spartina alterniflora* root dynamics in a Virginia marsh. *Marine Ecology Progress Series* 102: 169–178.

Blum, L.K., and R.R. Christian. 2004. Belowground production and decomposition along a tidal gradient in a Virginia salt marsh. In *The ecogeomorphology of tidal marshes*, ed. S. Fagherazzi, M. Marani, and L.K. Blum. https://doi.org/10.1029/CE059p0047.

Boesch, D.F., W.C.W.C. Boicourt, R.I. Cullather, T. Ezer, J. Galloway, and G.E., Z.P. Johnson, Kilbourne, K.H., M.L. Kirwan, R.E. Kopp, S. Land, M. Li, W. Nardin, C.K. Sommerfield, and W.V. Sweet. 2018. *Sea-level rise: Projections for Maryland 27*. Cambridge, MD: University of Maryland Center for Environmental Science.

Bouma, T.J., K. Hengst, B.P. Koutstaal, and J. van Soelen. 2003. Estimating root lifespan of two grasses at contrasting elevation in a salt marsh by applying vitality staining on roots from in-growth cores. *Plant Ecology* 165: 235–245.

Brouwer, R. 1962. Distribution of dry matter in the plant. *Netherlands Journal of Agricultural Science* 10: 361–376.

Buth, G.J.C., and L.A.C.J. Voesenek. 1987. Decomposition of standing and fallen litter of halophytes in a Dutch salt marsh. In *Vegetation between land and sea*, ed. A.H.L. Huiskes, C.W.P.M. Blom, and J. Rozema, 146–162. Dordrecht: Junk. https://doi.org/10.1007/978-94-009-4065-9_12.

Cahoon, D.R., J.C. Lynch, P. Hensel, R. Boumans, B.C. Perez, B. Segura, and J.W. Day Jr. 2002a. High-precision measurements of wetland sediment elevation: I. Recent improvements to the sedimentation-erosion table. *Journal of Sedimentary Research* 72: 730–733.

Cahoon, D.R., J.C. Lynch, B.C. Perez, B. Segura, R.D. Holland, C. Stelly, G. Stephenson, and P. Hensel. 2002b. High-precision

measurements of wetland sediment elevation: II. The rod surface elevation table. *Journal of Sedimentary Research* 72: 734–739.

Callaway, J.C., D.R. Cahoon, and J.C. Lynch. 2013. The surface elevation table–marker horizon method for measuring wetland accretion and elevation dynamics. *Methods in Biogeochemistry of Wetlands* 10: 901–917.

Cornwell, J.C., M.S. Owens, L.W. Staver, and J.C. Stevenson. 2020. Tidal marsh restoration at Poplar Island I: Transformation of estuarine sediments into marsh soils. *Wetlands* 40: 1673–1686.

Craft, C., S. Broome, and C. Campbell. 2002. Fifteen years of vegetation and soil development after brackish-water marsh creation. *Restoration Ecology* 10: 248–258.

Craft, C., J. Reader, J.N. Sacco, and S.W. Broome. 1999. Twenty-five years of ecosystem development of constructed *Spartina alterniflora* (Loisel.) marshes. *Ecological Applications* 9: 1405–1419.

Cronin, W.B. 2005. *The disappearing islands of the Chesapeake*. Baltimore: Johns Hopkins University Press ISBN 0-8018-7435-1.

Crosby, S.C., A. Angermeyer, J.M. Adler, M.D. Bertness, L.A. Deegan, N. Sibinga, and H.M. Leslie. 2017. *Spartina alterniflora* biomass allocation and temperature: Implications for salt marsh persistence with sea-level rise. *Estuaries and Coasts* 40: 213–223.

Darby, F.A., and R.E. Turner. 2008. Below- and aboveground biomass of *Spartina alterniflora*: Response to nutrient addition. *Estuaries and Coasts* 31: 326–334.

Davis, G.H. 1987. Land subsidence and sea level rise on the Atlantic Coastal Plain of the United States. *Environmental Geology and Water Sciences* 10: 67–80.

Dean, J., and E. Walter. 1974. Determination of carbonate and organic matter in calcareous sediments and sedimentary rocks by loss on ignition; comparison with other methods. *Journal of Sedimentary Research* 44: 242–248.

DeLaune, R.D., J.A. Nyman, and W.H. Patrick. 1994. Peat collapse, ponding and wetland loss in a rapidly submerging coastal marsh. *Journal of Coastal Research* 10: 1021–1030.

Drexler, J.Z., and C.S.d. Fontaine, and S. Deverel. 2009. The legacy of wetland drainage on the remaining peat in the Sacramento — San Joaquin Delta, California, USA. *Wetlands* 29: 372–386.

Eggleston, J., and J. Pope. 2013. Land subsidence and relative sea-level rise in the southern Chesapeake Bay region. *US Geological Survey Circular* 1392: 30.

Fragoso, G., and T. Spencer. 2008. Physiographic control on the development of *Spartina* marshes. *Science* 322: 1064–1064.

Gallagher, J.L. 1983. Seasonal patterns in recoverable underground reserves in *Spartina alterniflora* Loisel. *American Journal of Botany* 70: 212–215.

Gallagher, J.L., P.L. Wolf, and W.J. Pfeiffer. 1984. Rhizome and root growth rates and cycles in protein and carbohydrate concentrations in Georgia *Spartina alterniflora* Loisel. plants. *American Journal of Botany* 71: 165–169.

Gibson, K.D., J.B. Zedler, and R. Langis. 1994. Limited response of cordgrass (*Spartina foliosa*) to soil amendments in a constructed marsh. *Ecological Applications* 4: 757–767.

Godshalk, G.L., and R.G. Wetzel. 1978. Decomposition of aquatic angiosperms. *II. Particulate Components. Aquatic Botany* 5: 301–327.

Hemminga, M.A., C.J. Kok, and W. de Munck. 1988. Decomposition of *Spartina anglica* roots and rhizomes in a salt marsh of the Westerschelde Estuary. *Marine Ecology Progress Series* 48: 175–184.

Hodson, R.E., R.R. Christian, and A.E. Maccubbin. 1984. Lignocellulose and lignin in the salt marsh grass *Spartina alterniflora*: Initial concentrations and short-term, post-depositional changes in detrital matter. *Marine Biology* 81: 1–7.

Hutchinson, G.E. 1957. Concluding remarks. *Cold Spring Harbor Symposia on Quantitative Biology* 22: 415–442.

Iwasa, Y., and J. Roughgarden. 1984. Shoot/root balance of plants: Optimal growth of a system with many vegetative organs. *Theoretical Population Biology* 25: 78–105.

Krone, R.B. 1987. A method for simulating historic marsh elevations. In *Coastal Sediments*, 316–323. American Society of Civil Engineers.

McKee, K.L., and W.L. Patrick. 1988. The relationship of smooth cordgrass (*Spartina alterniflora*) to tidal datums: A review. *Estuaries* 11: 143–151.

Mendelssohn, I.A., and J.T. Morris. 2002. Eco-Physiological Controls on the Productivity of Spartina Alterniflora Loisel. In *Concepts and Controversies in Tidal Marsh Ecology*, ed. M.P. Weinstein and D.A. Kreeger, 59–80. Kluwer Academic Publishers.

Merino, J., D. Huval, and A. Nyman. 2010. Implication of nutrient and salinity interaction on the productivity of Spartina patens. *Wetlands Ecology and Management* 18: 111–117.

Miller, C.B., A.B. Rodriguez, M.C. Bost, B.A. McKee, and N.D. McTigue. 2022. Carbon accumulation rates are highest at young and expanding salt marsh edges. *Communications Earth & Environment* 3: 173.

Morris, J.T. 2006. Competition among marsh macrophytes by means of geomorphological displacement in the intertidal zone. *Estuarine Coastal and Shelf Science* 69: 395–402.

Morris, J.T., D.C. Barber, J.C. Callaway, R. Chambers, S.C. Hagen, C.S. Hopkinson, B.J. Johnson, P. Megonigal, S.C. Neubauer, T. Troxler, and C. Wigand. 2016. Contributions of organic and inorganic matter to sediment volume and accretion in tidal wetlands at steady state. *Earth's Future* 4: 110–121.

Morris, J.T., and W.B. Bowden. 1986. A mechanistic, numerical model of sedimentation, mineralization, and decomposition for marsh sediments. *Soil Science Society of America Journal* 50: 96–105.

Morris, J.T., D.R. Cahoon, J.C. Callaway, C. Craft, S.C. Neubauer, and N.B. Weston. 2021. Marsh equilibrium theory: Implications for responses to rising sea level. In *Salt Marshes: Function, Dynamics, and Stresses*, ed. D.M. FitzGerald and Z.J. Hughes, 157–177. Cambridge: Cambridge University Press.

Morris, J.T., and J.C. Callaway. 2018. Physical and biological regulation of carbon sequestration in salt marshes. In *A Blue Carbon Primer: The State of Coastal Wetland Carbon Science, Practice, and Policy*, ed. L. Windam-Meyers, S. Crooks, and T. Troxler, 67–79. CRC Press.

Morris, J.T., J.Z. Drexler, L.J.S. Vaughn, and A.H. Robinson. 2022. An assessment of future tidal marsh resilience in the San Francisco Estuary through modeling and quantifiable metrics of sustainability. *Frontiers in Environmental Science* 10: 1039143.

Morris, J.T., J. Edwards, S. Crooks, and E. Reyes. 2012. Assessment of carbon sequestration potential in coastal wetlands. In *Recarbonization of the Biosphere: Ecosystems and the Global Carbon Cycle*, ed. R. Lal, K. Lorenz, R.F. Hüttl, B.U. Schneider, and J. von Braun, 517–531. Netherlands, Dordrecht: Springer.

Morris, J.T., and A. Jensen. 1998. The carbon balance of grazed and nongrazed *Spartina anglica* saltmarshes at Skallingen, Denmark. *Journal of Ecology* 86: 229–242.

Morris, J.T., J.A. Langley, W.C. Vervaeke, N. Dix, I.C. Feller, P. Marcum, and S.K. Chapman. 2023. Mangrove trees outperform saltmarsh grasses in building elevation but collapse rapidly under high rates of sea-level rise *Earth's Future* 11: e2022EF00320.

Morris, J.T., G.P. Shaffer, and J.A. Nyman. 2013a. Brinson review: Perspectives on the influence of nutrients on the sustainability of coastal wetlands. *Wetlands* 33: 975–988.

Morris, J.T., P.V. Sundareshwar, C.T. Nietch, B. Kjerfve, and D.R. Cahoon. 2002. Responses of coastal wetlands to rising sea level. *Ecology* 83: 2869–2877.

Morris, J.T., and K. Sundberg. 2024. Responses of coastal wetlands to rising sea-level revisited: the importance of organic

production. *Estuaries and Coasts*. https://doi.org/10.1007/s12237-023-01313-8.

Morris, J.T., K. Sundberg, and C.S. Hopkinson. 2013b. Salt marsh primary production and its responses to relative sea level and nutrients in estuaries at Plum Island, Massachusetts, and North Inlet, South Carolina, USA. *Oceanography* 26: 78–84.

O'Connell, J., D. Mishra, M. Alber, and K. Byrd. 2021. BERM: a belowground ecosystem resiliency model for estimating *Spartina alterniflora* belowground biomass. *New Phytologist* 232: 425–439.

Odum, E.P. 1969. The strategy of ecosystem development: an understanding of ecological succession provides a basis for resolving man's conflict with nature. *Science* 164: 262–270.

Oppenheimer, M., B.C. Glavovic, J. Hinkel, and R.v.d. Wal, A.K. Magnan, A. Abd-Elgawad, R. Cai, M. Cifuentes-Jara, R.M. DeConto, T. Ghosh, J. Hay, F. Isla, B. Marzeion, B. Meyssignac, and Z. Sebesvari. 2019. Sea level rise and implications for low-lying islands, coasts and communities. In *IPCC Special Report on the Ocean and Cryosphere in a Changing Climate*, ed. H.-O. Pörtner, D.C. Roberts, V. Masson-Delmotte, P. Zhai, M. Tignor, E. Poloczanska, K. Mintenbeck, A. Alegría, M. Nicolai, A. Okem, J. Petzold, B. Rama, and N.M. Weyer, 321–445. Cambridge, UK and New York, NY: Cambridge University Press.

Owers, C.J., C.D. Woodroffe, D. Mazumder, and K. Rogers. 2022. Carbon storage in coastal wetlands is related to elevation and how it changes over time. *Estuarine, Coastal and Shelf Science* 267: 107775.

Park, S.E., L.R. Benjamin, and A.R. Watkinson. 2003. The theory and application of plant competition models: An agronomic perspective. *Annals of Botany* 92: 741–748.

Snedden, G.A., K. Cretini, and B. Patton. 2015. Inundation and salinity impacts to above- and belowground productivity in *Spartina patens* and *Spartina alterniflora* in the Mississippi River deltaic plain: Implications for using river diversions as restoration tools. *Ecological Engineering* 81: 133–139.

Staver, L.W., J.T. Morris, J.C. Cornwell, J.C. Stevenson, W. Nardin, P. Hensel, M.S. Owens, and A. Schwark. 2024. Elevation changes in restored marshes at Poplar Island, Chesapeake Bay, MD: I. Trends and drivers of spatial variability. *Estuaries and Coasts*. https://doi.org/10.1007/s12237-023-01319-2.

Staver, L.W., J.C. Stevenson, J.C. Cornwell, N.J. Nidzieko, K.W. Staver, M.S. Owens, L. Logan, C. Kim, and S.Y. Malkin. 2020. Tidal marsh restoration at Poplar Island: II. Elevation trends, vegetation development, and carbon dynamics. *Wetlands* 40: 1687–1701.

U.S. Army Corps of Engineers. 1996. *Poplar Island, Maryland environmental restoration project integrated feasibility report and environmental impact statement*, 654. Baltimore: U. S. Army Corps of Engineers, Baltimore District. https://hdl.handle.net/11681/37457.

U.S. Environmental Protection Agency, Chesapeake Bay Program. 2019. *Chesapeake Bay mean surface salinity (1985-2018), Map of means CB salinity*. Chesapeake Bay Program. https://www.chesapeakebay.net/what/maps/chesapeake-bay-mean-surface-salinity-1985-2018.

Weston, N.B., E. Rodriguez, B. Donnelly, E. Solohin, K. Jezycki, S. Demberger, L.A. Sutter, J.T. Morris, S.C. Neubauer, and C.B. Craft. 2023. Recent acceleration of wetland accretion and carbon accumulation along the U.S. East Coast. *Earth's Future* 11: e2022EF003037.

Wilson, J.O., R. Buchsbaum, I. Valiela, and T. Swain. 1986. Decomposition in salt marsh ecosystems: Phenolic dynamics during decay of litter of Spartina alterniflora. *Marine Ecology Progress Series* 29: 177–187.

Yellen, B., J. Woodruff, C. Ladlow, D.K. Ralston, S. Fernald, and W. Lau. 2021. Rapid tidal marsh development in anthropogenic backwaters. *Earth Surface Processes and Landforms* 46: 554–572.